



## Study of the iron(III)-modified clinoptilolite in the adsorption of phosphate from aqueous medium: mechanism and kinetics

Iva Kaplanec<sup>a</sup>, Aleksander Rečnik<sup>b</sup>, Gregor Mali<sup>c</sup>, Nevenka Rajič<sup>a,\*</sup>

<sup>a</sup>Faculty of Technology and Metallurgy, Karnegijeva 4, 11000 Belgrade, Serbia, Tel. +381 11 3370 503; Fax: +381 11 3370 387; emails: nena@tmf.bg.ac.rs (N. Rajič); ikaplanec@tmf.bg.ac.rs (I. Kaplanec)

<sup>b</sup>Jožef Stefan Institute, SI-1001 Ljubljana, Slovenia, Tel. +386 1 477 39 00; Fax: +386 1 251 93 85; email: aleksander.recnik@ijs.si

<sup>c</sup>Department of Inorganic Chemistry and Technology, National Institute of Chemistry, Hajdrihova 19, SI-1001 Ljubljana, Slovenia, Tel. +386 1 467 02 00; Fax: +386 1 476 03 00; email: gregor.mali@ki.si

Received 1 February 2017; Accepted 24 April 2017

### ABSTRACT

Clinoptilolite-rich tuff (Z) enriched with Fe(III) was studied in the removal of phosphate ions present in aqueous medium at pH = 6.5. Fe(III) modification was performed by a simple wet impregnation giving the product (FeZ) with about 18 wt% Fe. Transmission electron microscopy showed the presence of a flaky Fe(III) amorphous precipitate on the clinoptilolite sheets and a preserved clinoptilolite crystallinity. The modification increased the specific surface area from 28.6 to 140.3 m<sup>2</sup> g<sup>-1</sup>. FeZ effectively adsorbed phosphate, the removal rate at 298 K varying from 86% to 42.5% (for C<sub>0</sub> = 50 mg dm<sup>-3</sup> and C<sub>0</sub> = 400 mg dm<sup>-3</sup>). The sorption isotherms were in accord with the Langmuir model, giving for the Langmuir constant (R<sub>L</sub>) values in the range 0–1 that are characteristic of a favourable adsorption. The data for adsorption kinetics were best described by the pseudo-second-order model suggesting chemisorption as the phosphate sorption mechanism. Intra-particle diffusion was present in the adsorption, but it was not the rate-limiting step. A <sup>31</sup>P static spin-echo mapping nuclear magnetic resonance (NMR) measurement was performed for studying the phosphate–FeZ interaction. The results showed that the phosphate adsorption on FeZ proceeds through electrostatic interactions and covalent bonding, the latter being more pronounced.

**Keywords:** Clinoptilolite; Phosphate adsorption; Adsorption mechanism; <sup>31</sup>P NMR; Kinetics; TEM

### 1. Introduction

Natural clinoptilolite has been the most commonly used adsorbent in environmental remediation and restoration due to its abundance and availability [1,2]. This zeolite exhibits an open reticular structure characterized by (eight- and ten-membered ring) channels of up to 0.7 nm in diameter [3]. The channels are occupied by exchangeable alkali and alkaline earth cations and water molecules. Due to its cation-exchange behaviour, clinoptilolite has been particularly useful in the removal of different cations such as ammonium and heavy metal cations from aqueous media [4–9]. A very recent study

suggested that clinoptilolite is a promising agent for the reduction of seawater salinity [10]. The sorption ability of clinoptilolite can also be improved by different modification methods [11]. Recently, a coating of clinoptilolite onto a carbonaceous support was reported to increase the uptake of Cs ions from 55 to 120.9 mg g<sup>-1</sup> [12].

The negatively charged aluminosilicate framework causes clinoptilolite to be inappropriate for binding anionic species that are contaminants from industry or originate from natural releases. Modification of the clinoptilolite surface by metal oxides, hydroxides or cationic organic surfactants makes the clinoptilolite effective for adsorption of different anions, oxyanions or non-polar organics [13–16].

\* Corresponding author.

As an important element phosphorous is used in various fields from different industries to agriculture. Phosphate ions ( $\text{PO}_4^{3-}$ ,  $\text{H}_2\text{PO}_4^-$  and  $\text{HPO}_4^{2-}$ ) are also pollutants which are responsible for eutrophication in lakes, reservoirs and rivers [17], so that elevated phosphate concentrations have become a serious concern worldwide over the past decade. Various techniques for the phosphate removal based on physical, chemical or biological methods have been employed but most of them suffer from high operational costs or low efficiency. In order to preserve water resources a great attention has been focused onto adsorption since it is a cost-effective method in which a variety of materials can be applied. Natural and modified minerals such as illite [18], palygorskite [19], diatomite [20], goethite, akaganeite and lepidocrocite [21] have recently been studied in the adsorption of phosphate from aqueous media.

In this study, we modified a clinoptilolite-rich tuff with iron(III) and tested the obtained adsorbent in the phosphate removal at pH = 6.5. At this pH phosphorous is mainly presented as  $\text{H}_2\text{PO}_4^-$  and  $\text{HPO}_4^{2-}$  ions and is at the maximum of its availability to plants. The specific objectives of this research were: (1) to coat the clinoptilolite surface with oxo/hydroxo iron(III) species, (2) to characterize the obtained adsorbent, (3) to determine the equilibrium and kinetic parameters of adsorption and (4) to investigate the adsorption mechanism, that is, the interactions between phosphate ions and iron(III). Experimental facts regarding the interaction of Fe(III) present on the surface of mineral adsorbents with phosphate ions from aqueous media have been scarce in literature.

## 2. Experimental setup

### 2.1. Reagents and chemicals

Clinoptilolite-rich tuff (Z) was obtained from Zeodigest (Semnan deposit, Iran) and used as a starting material. According to the manufacturer, Z contains clinoptilolite as the major mineral phase (>80 mass%), and quartz (<7.5 mass%) and feldspars (<13 mass%) as mineral impurities. Particles between 63 and 100  $\mu\text{m}$  mesh were used in experiments, the choice being based on the results of previous studies [6–8,14–16] that found for this fraction the highest sorption ability. All chemicals used were analytical grade reagents. Deionized water was used throughout the experiments. The initial pH of the solutions was fixed at  $6.5 \pm 0.02$  by dropwise addition of 0.1/0.01 mol  $\text{dm}^{-3}$  HCl or 0.1/0.01 mol  $\text{dm}^{-3}$  NaOH.

### 2.2. Modification of zeolite

Prior to its use Z was washed several times with deionized water to remove water soluble impurities and dried to a constant mass in an oven at 80°C. Z was modified to a Fe(III)-containing form by using procedure given by Pavlovic et al. [14]. Z was mixed with a solution of  $\text{Fe}(\text{NO}_3)_3 \cdot 9\text{H}_2\text{O}$  (*pro analysis* (p.a.) Sigma-Aldrich, Germany) in an acetate buffer (pH = 3.6) and then pH of the suspension was adjusted to 7 by 0.1 M NaOH solution. After stirring at 70°C for 24 h, the solid (FeZ) was separated from suspension by centrifugation, washed several times with deionized water, centrifuged and dried at 80°C to a constant mass.

### 2.3. Phosphate adsorption experiments

Adsorption isotherms were determined at 298, 308 and 318 K using the batch method. 1.0 g of the FeZ was placed in 100.0  $\text{cm}^3$  of  $\text{KH}_2\text{PO}_4$  (p.a. Aldrich) of a chosen concentration. A phosphate concentration range of 50–400  $\text{mg dm}^{-3}$  was selected by estimating that the elevated phosphate concentrations in contaminated aqueous media can be expected in this range. The suspensions were shaken at about 100 rpm for 24 h in a thermostated water bath (Mettmert WPE 45). The phosphate-loaded solid (P–FeZ) was then recovered by filtration using 0.45- $\mu\text{m}$  membrane filter.

The rate of adsorption was studied at temperatures of 298, 308 and 318 K in solutions with an initial concentration of 50, 100, 200, 300 and 400  $\text{mg dm}^{-3}$ . The suspensions were shaken at a rate of about 100 rpm for a time period from 20 min to 24 h. The solid (P–FeZ) was then separated by filtration and the phosphate concentration was determined in filtrate.

All the experiments were carried out under controlled conditions: the temperature of the thermostated bath was maintained constant to within  $\pm 0.1^\circ\text{C}$ , the solid samples were weighted to four-digit accuracy, and the solution concentrations were determined with four-digit accuracy.

### 2.4. Post-treatment of P–FeZ

The P–FeZ samples (0.5 g) were suspended in 0.05 mol  $\text{dm}^{-3}$  NaOH solution (50.0  $\text{cm}^3$ ) and left under shaking for either 24 h or 2 months at room temperature. After the treatment, the solid was recovered by filtration, and pH of the filtrates was measured. The percentage of phosphate desorption was determined as the ratio of the phosphate amount in the solution and in the adsorbent.

### 2.5. Characterization

The size and morphology of the grains as well as the elemental analyses of the grains were studied by a scanning electron microscope JEOL JSM 6610LV. The samples were prepared by embedding grains in an epoxy film by a procedure previously described in detail [6]. An average elemental composition of the samples was obtained by data collection at 10 different  $\text{mm}^2$ -sized windows on the pellet surface. The accuracy of the method was  $\pm 3\%$ .

The initial and equilibrium phosphate concentrations in the supernatant were determined by a standard procedure using PhosVer 3 reagent and an UV–VIS spectrophotometer (Hach DR/2800). The amount of phosphate adsorbed by FeZ was calculated from the difference between the initial and final equilibrium phosphate concentration.

X-ray powder diffraction (XRD) patterns were recorded at room temperature on an APD2000 Ital Structure using Cu K $\alpha$  radiation (Cu K $\alpha_1$  radiation,  $\lambda = 1.5406 \text{ \AA}$ ). Thermal analysis was performed using a SDT Q-600 simultaneous differential scanning calorimetry (DSC) and thermogravimetric analysis (TGA) instrument (TA Instruments). The samples (~10 mg) were heated in a standard alumina sample pan (90 mL) from the room temperature to 800°C at a heating rate of 5°C  $\text{min}^{-1}$  under nitrogen with a flow rate of 0.1  $\text{dm}^3 \text{ min}^{-1}$ .

The specific surface area of Z and FeZ was determined by the nitrogen sorption method using an automatic sorption analyzer (Micrometrics ASAP 2020).

Transmission electron microscopy (TEM) studies were performed using a 200-kV TEM (JEM-2100 UHR, Jeol Inc., Tokyo, Japan) equipped with an ultra-high-resolution, objective-lens pole-piece having a point-to-point resolution of 0.19 nm. Electron diffraction patterns (EDPs) and TEM images of the sample were recorded by 2k charge-coupled device camera using Digital Micrograph™ (Gatan Inc., USA) as a user interface.

The  $^{31}\text{P}$  static spin-echo mapping NMR measurement was carried out on a 300 MHz Varian Unity Inova spectrometer equipped with a standard 5 mm Varian MAS NMR probe. Larmor frequency for the  $^{31}\text{P}$  nuclei was 122.64 MHz. The  $^{31}\text{P}$  spin-echo mapping NMR spectrum was obtained as a sum of a series of spin-echo spectra recorded at different irradiation frequencies [21–23]. The irradiation-frequency step was 40 kHz. Durations of the  $90^\circ$  and  $180^\circ$  pulses in the spin-echo experiment were 5.4 and 10.8  $\mu\text{s}$ , respectively, and the delay between the pulses was 25  $\mu\text{s}$ . Repetition delay between consecutive scans was 0.02 s, and was more than an order of magnitude longer than the spin-lattice relaxation time measured at 0 ppm. Number of scans for each individual spectrum was  $10^6$ . The frequency axis of the  $^{31}\text{P}$  spin-echo mapping NMR spectrum was reported relative to 1 M  $\text{H}_3\text{PO}_4$  (0 ppm).

### 3. Results and discussion

#### 3.1. Characterization of the adsorbent

XRD analysis of Z, FeZ and P-FeZ (patterns are given in supplementary material) confirmed that clinoptilolite is the major component in all three zeolite samples and that transformation of Z into FeZ as well as the phosphate adsorption onto FeZ did not affect the clinoptilolite crystallinity.

Chemical composition of the clinoptilolite phase of Z and FeZ obtained by energy dispersive spectroscopy (EDS) analysis as well as the water content of the samples obtained by thermogravimetric (TG) analysis are given in Table 1.

The Si/Al molar ratio is similar (about 4.5) for both samples confirming that the clinoptilolite lattice was not influenced by the modification process. It is evident that modification increased the iron content in zeolite from 0.21 to 18.1 wt%. The content of exchangeable cations changed but the decrease in their concentration is significantly lower than the increase of the iron content. This indicates that the modification process proceeded not only through an ion exchange but also through precipitation of iron(III) species.

The accumulated Fe(III) precipitate at the clinoptilolite surface caused an increase of the specific surface area from  $28.6 \text{ m}^2 \text{ g}^{-1}$  (Z) to  $140.3 \text{ m}^2 \text{ g}^{-1}$  (FeZ). According to the results of

Table 1  
Chemical composition (wt%) of the zeolite samples.

	Z	FeZ
Al	7.13	5.12
Si	33.2	23.8
Na	2.09	0.19
K	1.33	0.31
Ca	0.76	0.45
Fe	0.20	18.1
$\text{H}_2\text{O}^a$	13.0	15.8

<sup>a</sup>Loss of ignition at  $600^\circ\text{C}$ .

our previous work [16], the increase of the specific surface area could be explained by the formation of a second porous system (i.e., iron(III) oxide particles) at the surface of clinoptilolite.

Thermal analysis (Fig. 1) showed that the Fe(III) loading led to an increase of water content in FeZ (15.8 wt%) in comparison with Z (13.0 wt%) and that it affects the dehydration process. Dehydration of Z proceeded rather continuously in contrast to FeZ for which the differential thermogravimetric (DTG) curve displayed several maxima at about  $250^\circ\text{C}$ ,  $335^\circ\text{C}$  and  $511^\circ\text{C}$ . The maxima can be attributed to dehydration of amorphous iron oxide [24] suggesting that Fe(III) precipitate corresponds to amorphous iron(III) oxide.

The Fe(III) precipitate was studied in detail by TEM analysis (Fig. 2). Well crystalline clinoptilolite pseudo-hexagonal sheets covered with flaky amorphous Fe(III) precipitate on the surface are evident at a typical TEM image of FeZ (Fig. 1(a)). The EDP shows two diffraction rings ( $D_1 = 0.27 \text{ nm}$  and  $D_2 = 0.15 \text{ nm}$ ) that appear in the sample areas with higher density of the Fe-rich precipitate (Fig. 1(b)). There are no distinct spots within the rings that would indicate its crystallinity.

A representative TEM image of the phosphate-containing sample (P-FeZ) is given in Fig. 3. The precipitate at the clinoptilolite surface is amorphous (see the inset in Fig. 3)

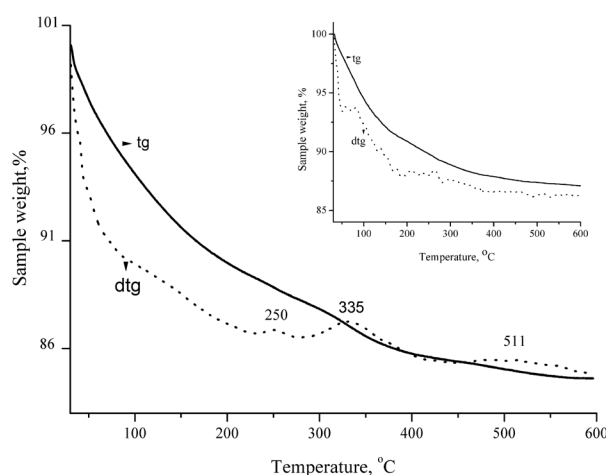


Fig. 1. TG/DTG curves of Z (inset) and FeZ.

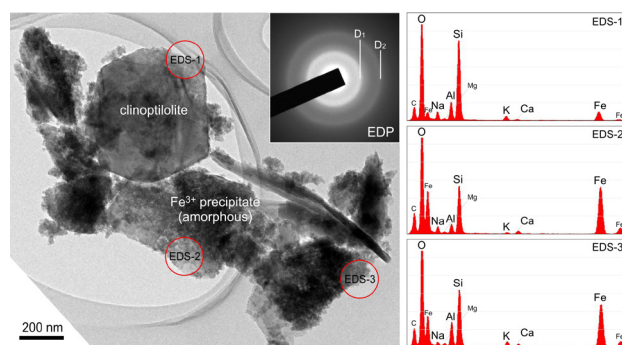


Fig. 2. (a) TEM study of FeZ sample: bright-field TEM image of clinoptilolite sheets covered with flaky Fe-rich precipitate. EDP (upper right corner) confirms that the precipitate is amorphous. (b) EDS analysis from areas indicated in the TEM image are shown on the right.

as in FeZ. In the sample areas that contain less Fe(III)-rich precipitate phosphorus is absent, appearing only where the amount of Fe(III) precipitate is higher (see EDS spectra). This shows that phosphate is bound to the Fe(III) precipitate rather than to clinoptilolite.

### 3.2. Adsorption experiments

Adsorption isotherms for phosphate on FeZ were studied at 298, 308 and 318 K (Fig. 4) showing that the adsorption capacity of FeZ increased both with temperature and with the initial phosphate solution concentration. FeZ effectively removed the phosphate ions from aqueous solutions at ambient temperature: adsorption capacity at 298 K varied from 4.3 mg g<sup>-1</sup> (for C<sub>0</sub> = 50 mg dm<sup>-3</sup>) to 17.0 mg g<sup>-1</sup> (for C<sub>0</sub> = 400 mg dm<sup>-3</sup>). Adsorption capacity increased with the increase of the phosphate concentration. There was a significant increase in adsorption capacity at 318 K: from 5.0 mg g<sup>-1</sup> (for C<sub>0</sub> = 50 mg dm<sup>-3</sup>) to 20.2 mg g<sup>-1</sup> (for C<sub>0</sub> = 400 mg dm<sup>-3</sup>).

The equilibrium data from Fig. 4 were analyzed using common isotherms – Langmuir, Freundlich, Temkin and Dubinin–Radushkevich [25].

The Langmuir model gave the most satisfactory fit (Table 2). The model assumes that: the adsorption occurs in monolayer, all surface sites are equivalent, and adsorption to one site does not depend on the adjacent sites occupancy [25]. The important characteristics of the Langmuir isotherm can be described by a separation factor  $R_L$ , defined as Eq. (1) [25]:

$$R_L = \frac{1}{1 + b_L C_0} \quad (1)$$

where C<sub>0</sub> is the initial phosphate concentration and b<sub>L</sub> is the Langmuir constant. The dimensionless constant,  $R_L$ , is used to express the favourability of the adsorption: 0 <  $R_L$  < 1 indicates favourable adsorption,  $R_L$  > 1 assumes unfavourable adsorption,  $R_L$  = 1 is for linear adsorption and  $R_L$  = 0 suggests irreversible adsorption [25]. Values of  $R_L$  here are in the 0–1 range (given in supplementary material) indicating favourable phosphate adsorption on FeZ.

The adsorption capacities of FeZ are rather difficult to compare with those reported for different materials because

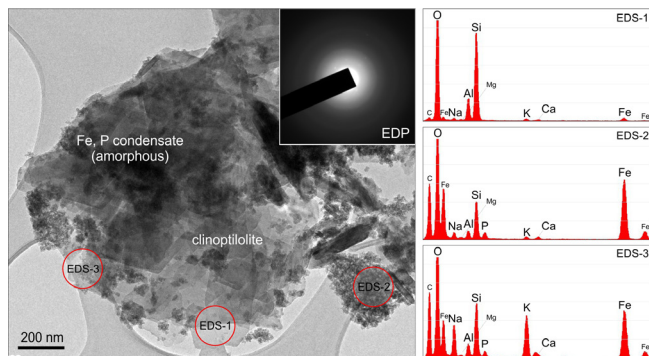


Fig. 3. (a) TEM image of P-FeZ. EDP (inset) indicates that the phosphate-containing precipitate is amorphous. (b) EDS analysis recorded from the areas marked in the TEM image shows an increase of the P–K peak with Fe–K stemming from the Fe-rich precipitate.

of differing experimental conditions (initial phosphate concentration, temperature, grain size, contact time and pH). Generally, monolayer phosphate adsorption obtained in this research is in accord with the Langmuir isotherm model reported for the phosphate adsorption on different iron-oxide-based adsorbents [26] and on a Fe–Al–hydrogel derived from bentonite [27] in a similar range of initial

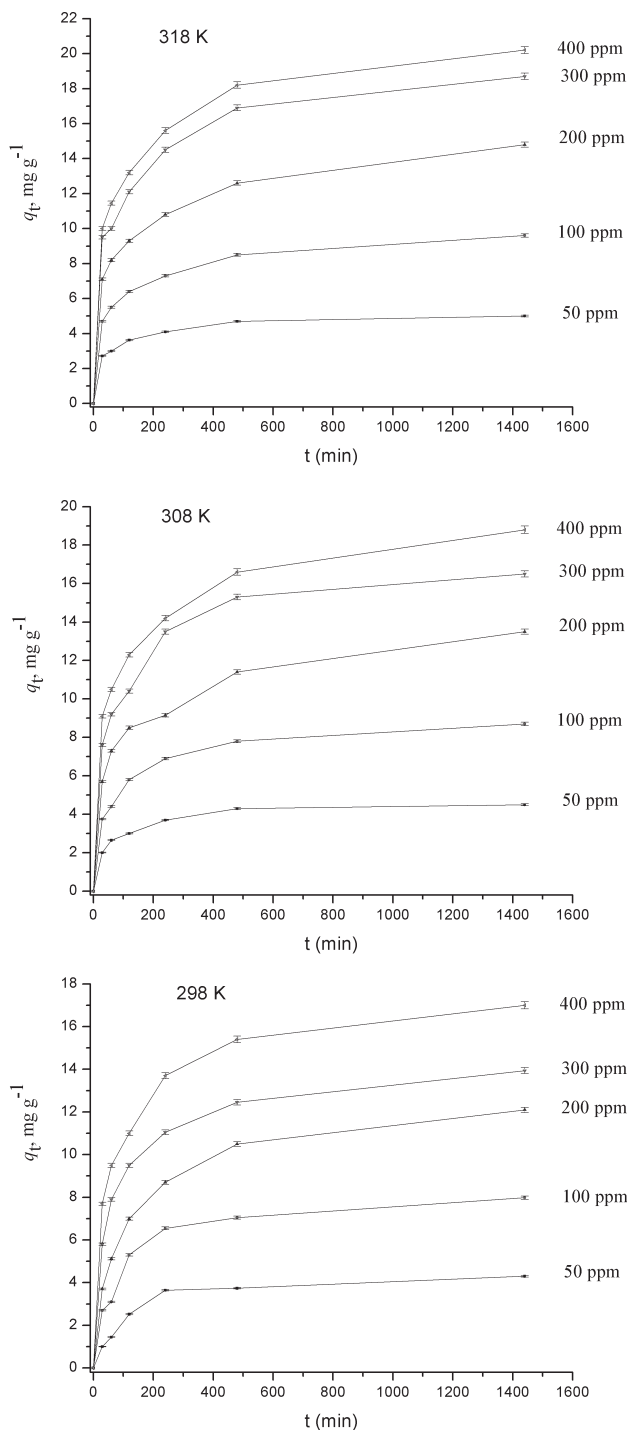


Fig. 4. Adsorption kinetics for phosphate on FeZ for different initial phosphate concentrations;  $q_t$  is the amount of the adsorbed phosphate (mg per 1 g of FeZ) after time  $t$ .

phosphate concentrations and at nearly neutral pH. Moreover, for initial concentration of 100 mg dm<sup>-3</sup> and pH ~7 and at 298 K the adsorption capacity reported for the acid-treated palygorskite (6.6 mg g<sup>-1</sup>) [28] is lower than that for FeZ (8.2 mg g<sup>-1</sup>). The adsorption capacity of the Fe–Al–hydrogel [27] was reported as 14.29 mg g<sup>-1</sup> for initial phosphate concentrations from 10 to 1,000 mg dm<sup>-3</sup> at pH ~6.5 which is significantly lower than the capacity of FeZ is at all studied temperatures for the initial concentration of 400 mg dm<sup>-3</sup> (17.0–20.2 mg g<sup>-1</sup>). The adsorption capacity of FeZ at 298 K and for the initial concentration of 400 mg dm<sup>-3</sup> is also higher than that reported for the aluminium hydroxide modified palygorskite nano-composites for the initial concentration of 500 mg dm<sup>-3</sup> at pH ~5 (16.04 mg g<sup>-1</sup>) [19].

### 3.3. Kinetic analysis

The time dependence of the phosphate adsorption was studied at 298, 308 and 318 K for solutions with  $C_0 = 50, 100, 200, 300$  and  $400$  mg dm<sup>-3</sup>. This dependence on time was followed until the adsorption equilibrium has practically been reached, which occurred in around 24 h. Fig. 4 shows the progress of the phosphate adsorption from solution.

Fig. 4 shows that at the early stages of adsorption (i.e., approximately in the first 100 min), the phosphate adsorption increases quite steeply from  $q_t = 0$  at  $t = 0$ . Subsequently, the adsorption occurs more slowly. Similar behaviour was reported for the goethite-based adsorbents [26].

The data shown in Fig. 4 were examined using three kinetic models, two of them being reaction-based and the

third one diffusion-based [29–31]. The first reaction-based model was Lagergren's first-order rate Eq. (2) [29]:

$$\frac{dq_t}{dt} = k_1(q_e - q_t) \quad (2)$$

where  $q_e$  (mg g<sup>-1</sup>) being the adsorption capacity at equilibrium and  $k_1$  (min<sup>-1</sup>) the rate constant of the first-order adsorption. Lagergren's first-order rate equation is often referred to as the pseudo-first-order rate equation [29,30] in order to tell apart kinetic expressions based on concentrations of solution and those based on adsorption capacities of solids. Integration of the expression (2) between the limits  $t = 0$  to  $t = t$  and  $q = 0$  to  $q = q_t$  gives Eq. (3):

$$\log(q_e - q_t) = \log q_e - \frac{k_1}{2.303} t \quad (3)$$

If the experimental data match the kinetic model (3), the plot of  $\log(q_e - q_t)$  vs.  $t$  results in a straight line.

The second reaction-based model applied to the data from Fig. 4 was the pseudo-second-order model which is defined by the following rate equation [30]:

$$\frac{dq_t}{dt} = k_2(q_e - q_t)^2 \quad (4)$$

where  $k_2$  (g mg<sup>-1</sup> min<sup>-1</sup>) being the rate constant of the pseudo-second-order adsorption. Integrating between the same limits as for Eq. (3) gives Eq. (5):

Table 2  
Isotherm parameters for the phosphate adsorption on FeZ at 298, 308 and 318 K

Isotherm	Equation	Temperatures, K		
		298	308	318
Langmuir	$q_e = \frac{q_{\max} b_L C_e}{1 + b_L C_e}$			
$q_e$ , mg g <sup>-1</sup>		18.60	20.68	21.27
$b_L$ , dm <sup>3</sup> mg		0.03	0.04	0.06
$R^2$		0.9904	0.9957	0.9961
Freundlich	$q_e = K_F C_e^{b_F}$			
$K_F K_F'$ , [mg g <sup>-1</sup> (dm <sup>3</sup> mg <sup>-1</sup> ) <sup>b<sub>F</sub></sup> ]		2.06	2.52	4.20
$b_F$		2.58	2.62	3.3
$R^2$		0.9818	0.9729	0.9974
Temkin	$q_e = B_T \ln A_T + B_T \ln C_e$ , $B_T = \frac{RT}{b_T}$			
$A_T$ , dm <sup>3</sup> g <sup>-1</sup>		0.37	0.49	1.82
$B_T$		3.6	3.92	3.32
$R^2$		0.9909	0.9947	0.9916
Dubinin–Radushkevich	$q_e = \ln q_D - 2K_D RT \ln \left( 1 + \frac{1}{C_e} \right)$			
$K_D$ , mol <sup>2</sup> kJ <sup>-2</sup>		$1.76 \times 10^{-5}$	$1.09 \times 10^{-5}$	$9.93 \times 10^{-7}$
$q_D$ , mg g <sup>-1</sup>		13.21	15.21	15.43
$R^2$		0.9282	0.9478	0.8789

$$\frac{t}{q_t} = \frac{1}{k_2 q_e^2} + \frac{1}{q_e} t \quad (5)$$

If the experimental data correspond to the pseudo-second-order model the plot of  $t/q_t$  vs.  $t$  yields a straight line. From the slope and intercept of the plot, respectively, the values of  $q_e$  and  $k_2$  can be evaluated.

Table 3 lists the results obtained by applying the two models on the experimental data. It is seen that Lagergren's second-order model gives an excellent agreement as the determination coefficient ( $R^2$ ) of the linear regression is very close to 1 for all studied initial concentrations and temperatures. This model is in accord with a monolayer adsorption, confirming the result obtained by adsorption isotherms.

### 3.3.1. Diffusion effects

The experimental data were further analyzed by the Weber–Morris mass transfer model [32] in order to see to which extent diffusion participates in the adsorption process. The Weber–Morris model is described by Eq. (6):

$$q_t = k_d t^{1/2} + I \quad (6)$$

where  $q_t$  ( $\text{mg g}^{-1}$ ) being the adsorption capacity at time  $t$  (min),  $k_d$  ( $\text{mg g}^{-1} \text{min}^{-1/2}$ ) is the diffusion rate constant and  $I$  ( $\text{mg g}^{-1}$ ) is the intercept at the ordinate.

Fig. 5 shows the plots of  $q_t$  vs.  $t^{1/2}$  for various temperatures and various initial phosphate concentrations. It is seen that the plots are straight lines which consist of two segments: the first segment, with a steeper slope, lies in the  $t^{1/2}$  region up to about  $15 \text{ min}^{1/2}$  while the second one is located at higher

Table 3  
Pseudo-second-order kinetic parameters for the phosphate adsorption on the FeZ

$C_0, \text{mg dm}^{-3}$	$q_e, \text{mg g}^{-1}$	$k_2, \text{g mg}^{-1} \text{h}^{-1}$	$R^2$
298 K			
50	4.64	0.0018	0.9995
100	8.40	0.0015	0.9996
200	12.85	0.0008	0.9996
300	14.4865	0.0011	0.9997
400	17.62	0.0008	0.9996
308 K			
50	4.65	0.0039	0.9997
100	9.04	0.0017	0.9997
200	14.10	0.00087	0.9980
300	17.18	0.00093	0.9994
400	19.49	0.0008	0.9992
318 K			
50	5.14	0.0044	0.9997
100	9.94	0.0016	0.9992
200	15.38	0.0009	0.9986
300	19.41	0.00084	0.9994
400	20.94	0.00081	0.9994

$t^{1/2}$  values. The second segment is usually assigned to the intra-particle diffusion. This segment was analyzed by linear regression and in all cases the intercept  $I$  (Eq. (6)) was found to be greater than zero. The fact that  $I > 1$  shows [32] that the intra-particle diffusion is not the rate-limiting step in the studied system.

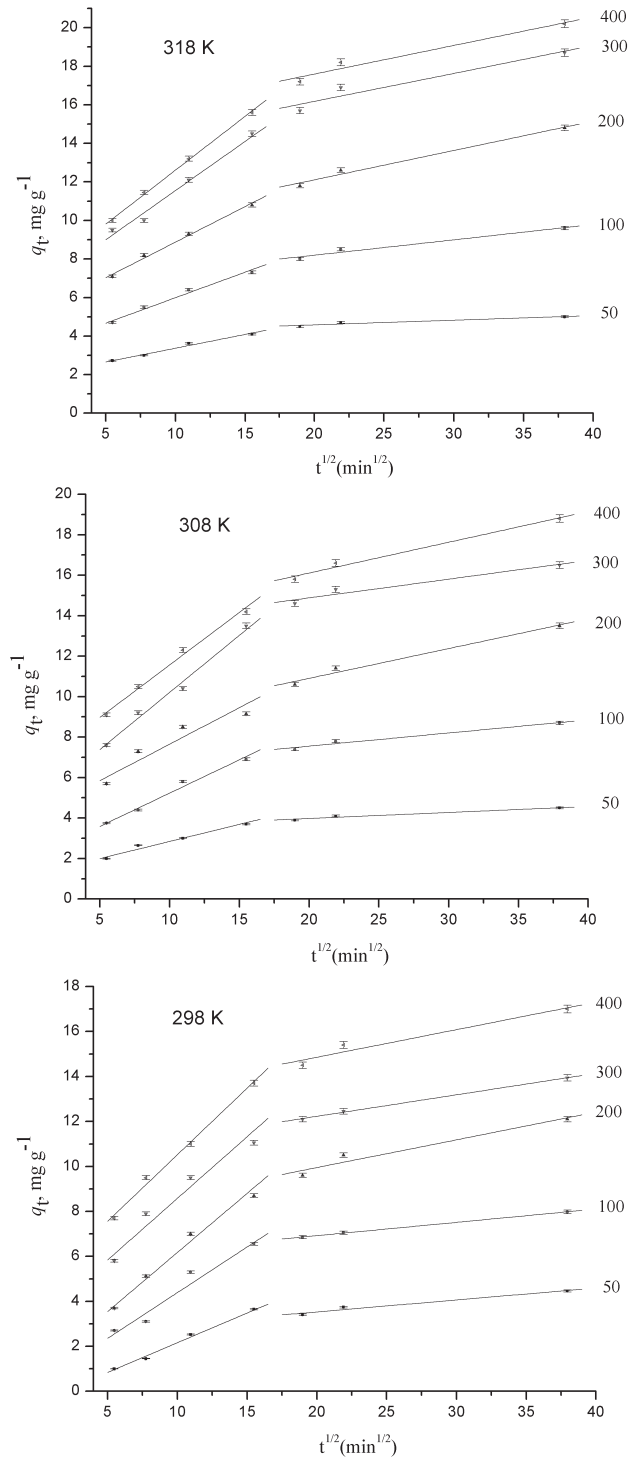


Fig. 5. Intra-particle diffusion kinetics for phosphate adsorption on FeZ according to the Weber–Morris mass transfer model.

The present kinetic results were in accordance with the pseudo-second order model which has been reported as the most acceptable in describing kinetics of the phosphate adsorption on other natural materials such as clays [33], modified clays [19,34], oxides [26] and synthetic zeolite [33]. The calculated adsorbed amounts at equilibrium are very close to the experimental values for all studied temperatures and initial concentrations. Moreover, for FeZ as well as for the aluminium hydroxide modified palygorskite [19] the intra-particle diffusion analysis suggested that such diffusion is not the rate-limiting step in the phosphate adsorption. This is in contrast to the results reported for a commercial goethite-based adsorbent [26].

### 3.4. Desorption experiment

The phosphate leaching was studied using P-FeZ which had the phosphate content of 19 mg g<sup>-1</sup>. Desorption rate in 0.05 M NaOH was about 30% after 24 h reaching 40% after 2 months and being accompanied with a slight increase of pH from 7.7 to 7.9 during the treatment. The observed desorption rate indicates that phosphate ions mainly form strong bonds with FeZ. A similar conclusion was reported for the role of FeZ in the prevention of phosphate leaching from soils [35]. Moreover, the present results are comparable with those obtained for phosphate desorption from a commercial goethite-based adsorbent (E33) and its Mn- and Ag-coated forms [26].

### 3.5. <sup>31</sup>P NMR studies

In order to get a deeper insight into the phosphate-FeZ interaction, <sup>31</sup>P NMR analysis was performed on P-FeZ. <sup>31</sup>P NMR has already been employed for studying adsorption of phosphate on iron(III)-containing materials. Kim et al. [21] thoroughly investigated phosphate adsorption on the surfaces of iron-oxyhydroxide polymorphs goethite, akaganeite and lepidocrocite, and concluded that phosphate anions predominantly bind to these polymorphs through two covalent P-O-Fe bonds. The existence of such bonds was reflected in very large <sup>31</sup>P hyperfine shifts of the <sup>31</sup>P NMR signals. The shifts of several hundred to several thousand ppm were due to the strong through-bond hyperfine interactions between the <sup>31</sup>P nuclear spins and the spins of the unpaired electrons of the paramagnetic Fe<sup>3+</sup> centers. Strong electron-nucleus through-space spin-spin interactions also lead to very broad lines, which needed to be recorded by frequency sweeping spin-echo mapping technique. The <sup>31</sup>P spin-echo mapping NMR spectrum of P-FeZ is shown in Fig. 6. The spectrum exhibits a broad signal, or, more probably, a set of overlapping broad signals, extending between ca. 5,500 and -1,000 ppm. Although the signal-to-noise ratio of the <sup>31</sup>P NMR spectrum of P-FeZ is quite low, four to five peak maxima can be identified in the spectrum. The sharpest peak with its maximum close to 0 ppm is not shifted by the hyperfine interaction and can be ascribed to phosphate units that do not form covalent P-O-Fe bonds. They belong to the so-called outer-sphere phosphate complexes or physisorbed phosphate anions which electrostatically interact with the FeZ surface. All other signals are severely shifted and thus indicate that the majority (about 85%) of the phosphate adsorbed

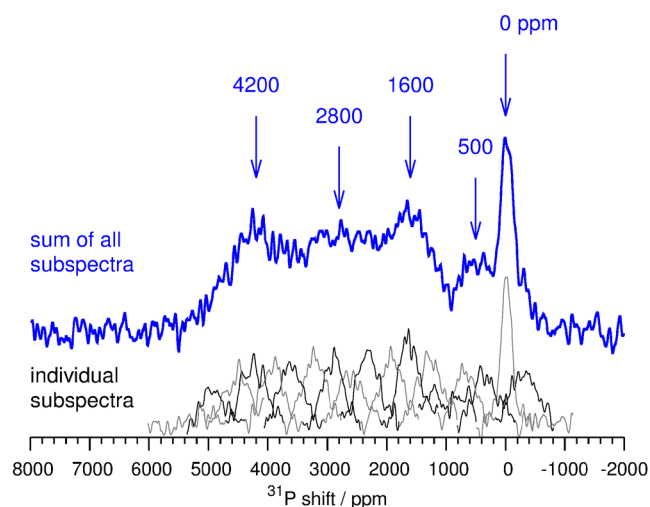


Fig. 6. The spin-echo-mapping <sup>31</sup>P NMR spectrum of P-FeZ.

to FeZ is covalently bound to the surface of the Fe(III) precipitate found by TEM analysis. Because the Fe(III) precipitate is amorphous the observed peak maxima cannot be directly compared with those detected for the phosphate adsorbed on crystalline goethite (peak maximum at 2,650 ± 200 ppm), akaganeite (1,100 ± 200 ppm), or lepidocrocite (2,800 ± 200 ppm) [21]. Still, from the approximate peak positions it can be suggested that a large fraction of phosphate ions form two P-O-Fe bonds with the iron(III) species, because the observed hyperfine shifts are as large as or even larger than the ones detected in the case of the phosphate adsorbed on the crystalline iron-oxyhydroxide polymorphs. It should be noted that the magnitude of the hyperfine coupling on the <sup>31</sup>P nucleus is roughly proportional to the number of P-O-Fe covalent bonds to this nucleus and that larger hyperfine shifts correspond to a larger number of covalent bonds. Vice versa, smaller number of covalent bonds lead to smaller <sup>31</sup>P hyperfine shifts, which means that a part of the <sup>31</sup>P NMR spectrum of P-FeZ, in particular the part with the peak maximum at about 500 ppm, can be assigned also to monodentately bound phosphates complexes. In summary, the <sup>31</sup>P NMR spectroscopy thus undoubtedly confirms that in P-FeZ the majority of phosphate species are covalently bound to the surface of iron(III) species.

## 4. Conclusion

Fe(III)-containing clinoptilolite with about 18 wt% Fe is an efficient adsorbent for phosphate ions present in water medium at pH ~6.5. The adsorption capacity increases with temperature and initial concentration. The adsorption isotherm is in accord with the Langmuir model, giving for the Langmuir constant ( $R_L$ ) values characteristic of a favourable adsorption. The adsorption kinetics is best described by the pseudo-second-order model suggesting chemisorption for the phosphate adsorption mechanism. Intra-particle diffusion studies indicated that the phosphate adsorption occurs in two stages and that intra-particle diffusion is not the rate-limiting step.

TEM and <sup>31</sup>P NMR analyses showed that the phosphate adsorption occurs at the Fe(III)-coating present on the

clinoptilolite sheets. The adsorption mechanism includes two types of interactions: electrostatic and covalent bonding. The covalent bonds are more prominent and they include the phosphate bonding to Fe(III) predominantly as a bidentate ligand.

### Acknowledgements

This study was funded by the Ministry of Education, Science and Technological Development of the Republic of Serbia (Project No. 172018). The authors are very grateful to the Zeodigest Company from Iran for providing zeolitic tuff samples.

### Symbols

$K$	—	Equilibrium constant
$q_t$	—	Amount of the adsorbed phosphate after time $t$ , mg g <sup>-1</sup>
$q_e$	—	Amount of the adsorbed phosphate at equilibrium, mg g <sup>-1</sup>
$t$	—	Time, min
$q_{\max}$	—	Langmuir constant related to the maximum achievable uptake by a system, mg g <sup>-1</sup>
$b_L$	—	Langmuir isotherm constant, dm <sup>3</sup> mg <sup>-1</sup>
$b_F$	—	Freundlich isotherm constant
$A_T$	—	Temkin isotherm equilibrium binding constant, dm <sup>3</sup> g <sup>-1</sup>
$b_T$	—	Temkin isotherm constant
$B_T$	—	Temkin constant related to heat of sorption, J mol <sup>-1</sup>
$K_D$	—	Dubinin–Radushkevich constant related to free energy of sorption, mol <sup>2</sup> kJ <sup>-2</sup>
$q_D$	—	Dubinin–Radushkevich model constant, mg g <sup>-1</sup>
$C_e$	—	Concentration of the phosphate solution at equilibrium, mg dm <sup>-3</sup>
$C_0$	—	Initial concentration of the phosphate solution, mg dm <sup>-3</sup>
$I$	—	Intercept at the ordinate in the Weber–Morris model, mg g <sup>-1</sup>
$k_2$	—	The rate constant of the pseudo-second-order model, g mg <sup>-1</sup> h <sup>-1</sup>
$k_d$	—	The diffusion rate constant, mg g <sup>-1</sup> min <sup>-1/2</sup>
$R$	—	Universal gas constant, 8.314 J mol <sup>-1</sup> K <sup>-1</sup>
$R^2$	—	Coefficient of determination

### References

- [1] P. Misaelides, Application of natural zeolites in environmental remediation: a short review, *Microporous Mesoporous Mater.*, 144 (2011) 15–18.
- [2] E. Chmielewska, *Environmental Zeolites and Aqueous Media: Examples of Practical Solution*, Bentham Science Publishers, Sharjah, 2014.
- [3] A. Godelitsas, T. Armbruster, HEU-type zeolites modified by transition elements and lead, *Microporous Mesoporous Mater.*, 61 (2003) 3–24.
- [4] J. Milovanovic, S. Eich-Greatorex, T. Krogstad, V. Rakic, N. Rajic, The use in grass production of clinoptilolite as an ammonia adsorbent and a nitrogen carrier, *J. Serb. Chem. Soc.*, 80 (20015) 1203–1214.
- [5] N. Rajic, D. Stojakovic, S. Jevtic, N. Zabukovec Logar, M. Mazaj, V. Kaucic, Removal of aqueous manganese using the natural zeolitic tuff from the Vranjska Banja deposit in Serbia, *J. Hazard. Mater.*, 172 (2010) 1450–1457.
- [6] N. Rajic, D. Stojakovic, M. Jovanovic, N. Zabukovec Logar, M. Mazaj, V. Kaucic, Removal of nickel(II) ions from aqueous solutions using the natural clinoptilolite and preparation of nano-NiO on the exhausted clinoptilolite, *Appl. Surf. Sci.*, 257 (2010) 1524–1532.
- [7] D. Stojakovic, J. Milenkovic, N. Daneu, N. Rajic, A study of the removal of copper ions from aqueous solution using clinoptilolite from Serbia, *Clays Clay Miner.*, 59 (2011) 277–285.
- [8] D. Stojakovic, J. Hrenovic, M. Mazaj, N. Rajic, On the zinc sorption by the Serbian natural clinoptilolite and the disinfecting ability and phosphate affinity of the exhausted sorbent, *J. Hazard. Mater.*, 185 (2011) 408–415.
- [9] E. Chmielewska, Natural zeolite – a versatile commodity – some retrospectives in water cleanup processes, *Desal. Wat. Treat.*, 41 (2012) 335–341.
- [10] E. Wibowo, M. Rokhmat, S. Khairurrijal, M. Abdullah, Reduction of seawater salinity by natural zeolite (clinoptilolite): adsorption isotherms, thermodynamics and kinetics, *Desalination*, 409 (2017) 146–156.
- [11] A. Günaj, E. Arslankaya, İ. Tosun, Lead removal from aqueous solution by natural and pretreated clinoptilolite: adsorption equilibrium and kinetics, *J. Hazard. Mater.*, 146 (2007) 362–371.
- [12] D.A. De Haro-Del Rio, S. Al-Joubori, O. Kontogiannis, D. Papadatos-Gigantes, O. Ajayi, C. Li, S.M. Holmes, The removal of caesium ions using supported clinoptilolite, *J. Hazard. Mater.*, 289 (2015) 1–8.
- [13] Z. Li, J.S. Jean, W.T. Jiang, P.H. Chang, C.J. Chen, L. Liao, Removal of arsenic from water using Fe-exchanged natural zeolite, *J. Hazard. Mater.*, 187 (2011) 318–323.
- [14] J. Pavlovic, J. Milenkovic, N. Rajic, Modification of natural clinoptilolite for nitrate removal from aqueous media, *J. Serb. Chem. Soc.*, 79 (2014) 1309–1322.
- [15] V. Rakić, N. Rakić, A. Daković, A. Auroux, The adsorption of salicylic acid, acetylsalicylic acid and atenolol from aqueous solutions onto natural zeolites and clays: clinoptilolite, bentonite and kaolin, *Microporous Mesoporous Mater.*, 166 (2013) 185–194.
- [16] S. Jevtić, I. Arčon, A. Rečnik, B. Babić, M. Mazaj, J. Pavlović, D. Matijašević, M. Nikšić, N. Rakić, The iron(III)-modified natural zeolitic tuff as an adsorbent and carrier for selenium oxyanions, *Microporous Mesoporous Mater.*, 197 (2014) 92–100.
- [17] D.L. Correll, The role of phosphorus in the eutrophication of receiving waters: a review, *J. Environ. Qual.*, 27 (1998) 261–266.
- [18] K. Adam, A.K. Søvik, T. Krogstad, Sorption of phosphorus to Filtralite-P™ – the effect of different scales, *Water Res.*, 40 (2006) 1143–1154.
- [19] M. Pan, X. Lin, J. Xie, X. Huang, Kinetic, equilibrium and thermodynamic studies for phosphate adsorption on aluminum hydroxide modified palygorskite nano-composites, *RSC Adv.*, 7 (2017) 4492–4500.
- [20] P. Xia, X. Wang, X. Wang, J. Song, H. Wang, J. Zhang, J. Zhao, Struvite crystallization combined adsorption of phosphate and ammonium from aqueous solutions by mesoporous MgO-loaded diatomite, *Colloids Surf., A*, 506 (2016) 220–227.
- [21] J. Kim, W. Li, B.L. Philips, C.P. Grey, Phosphate adsorption on the iron oxyhydroxides goethite ( $\alpha$ -FeOOH), akaganeite ( $\beta$ -FeOOH), and lepidocrocite ( $\gamma$ -FeOOH): a <sup>31</sup>P NMR study, *Energy Environ. Sci.*, 4 (2011) 4298–4305.
- [22] G. Mali, A. Ristić, V. Kaučić, <sup>31</sup>P NMR as a tool for studying incorporation of Ni, Co, Fe, and Mn into aluminophosphate zeotypes, *J. Phys. Chem. B*, 109 (2005) 10711–10716.
- [23] Y.Y. Tong, Nuclear spin-echo Fourier-transform mapping spectroscopy for broad NMR lines in solids, *J. Magn. Reson., Ser. A*, 119 (1996) 22–28.
- [24] N.D. Phu, D.T. Ngo, L.H. Hoang, N.H. Luong, N. Chau, N.H. Hai, Crystallization process and magnetic properties of amorphous iron oxide nanoparticles, *J. Phys. D: Appl. Phys.*, 44 (2011) 345002.
- [25] K. Vijayaraghavan, T.V.N. Padmesh, K. Palanivelu, M. Velan, Biosorption of nickel(II) ions onto *Sargassum wightii*: application of two-parameter and three-parameter isotherm models, *J. Hazard. Mater.*, 133 (2006) 304–308.

- [26] J. Lalley, C. Han, X. Li, D.D. Dionysiou, M.N. Nadagouda, Phosphate adsorption using modified iron oxide-based sorbents in lake water: kinetics, equilibrium, and column tests, *Chem. Eng. J.*, 284 (2016) 1386–1396.
- [27] S.Z. Rahni, N. Mirghaffari, B. Rezaei, H.S. Ghaziaskar, Removal of phosphate from aqueous solutions using a new modified bentonite-derived hydrogel, *Water Air Soil Pollut.*, 225 (2014) 1916.
- [28] H. Ye, F. Chen, Y. Sheng, G. Sheng, J. Fu, Adsorption of phosphate from aqueous solution onto modified palygorskites, *Sep. Purif. Technol.*, 50 (2006) 283–290.
- [29] S. Lagergren, Zur theorie der sogenannten adsorption gelöster stoffe, *K. Sven. Vetensk.akad. Handl.*, 24 (1898) 1–39.
- [30] Y.S. Ho, Review of second-order models for adsorption systems, *J. Hazard. Mater.*, 136 (2006) 681–689.
- [31] Y.S. Ho, G. McKay, Pseudo-second order model for sorption processes, *Process Biochem.*, 34 (1998) 451–465.
- [32] W.J. Weber Jr., J.C. Morris, Kinetics of adsorption on carbon from solution, *J. Sanit. Eng. Div. Proc. Am. Soc. Civil Eng.*, 89 (1963) 31–60.
- [33] N. Hamdi, E. Srasra, Removal of phosphate ions from aqueous solution using Tunisian clays minerals and synthetic zeolite, *J. Environ. Sci.*, 24 (2012) 617–623.
- [34] L.G. Yan, Y.Y. Xu, H.Q. Yu, X.D. Xin, Q. Wei, B. Du, Adsorption of phosphate from aqueous solution by hydroxy-aluminum, hydroxy-iron and hydroxy-iron–aluminum pillared bentonites, *J. Hazard. Mater.*, 179 (2010) 244–250.
- [35] I. Pavlovic, T. Krogstad, N. Rajic, Influence of the Fe(III)-modified clinoptilolite on phosphorus leaching from different soil types, *J. Mat. Prot.*, 57 (2016) 539–544.

## Supplementary material

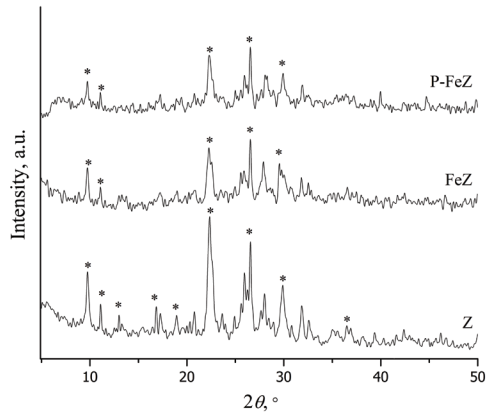


Fig. S1. XRD patterns of Z, FeZ and P-FeZ.

Table S1

Values of the separation factor ( $R_L$ ) for different initial concentration of phosphate ions and different temperatures

$C_0$ , mg dm <sup>-3</sup>	$R_L$		
	298 K	308 K	318 K
50	0.4000	0.3333	0.2500
100	0.2500	0.2000	0.1429
200	0.1429	0.1111	0.0770
300	0.1000	0.0770	0.0526
400	0.0770	0.0588	0.0400